

Designing Interpretable Approximations to Deep Reinforcement Learning with Soft Decision Trees

Nathan Dahlin, Krishna Chaitanya Kalagarla, Nikhil Naik, Rahul Jain, Pierluigi Nuzzo

University of Southern California
3740 McClintock Avenue, Los Angeles, CA 90089-2560

Abstract

In an ever expanding set of research and application areas, deep neural networks (DNNs) set the bar for algorithm performance. However, depending upon additional constraints such as processing power and execution time limits, or requirements such as verifiable safety guarantees, it may not be feasible to actually use such high-performing DNNs in practice. Many techniques have been developed in recent years to *compress* or *distill* complex DNNs into smaller, faster or more understandable models and controllers. This work seeks to provide a quantitative framework with metrics to systematically evaluate the outcome of such conversion processes, and identify reduced models that not only preserve a desired performance level, but also, for example, succinctly explain the latent knowledge represented by a DNN. We illustrate the effectiveness of the proposed approach on the evaluation of decision tree variants in the context of benchmark reinforcement learning tasks.

1 Introduction

Deep neural network (DNN)-driven algorithms now stand as the state of the art in a variety of domains, from perceptual tasks such as computer vision, speech and language processing to, more recently, control tasks such as robotics (Mirzadeh et al. 2019), (Bastani, Pu, and Solar-Lezama 2018). Nevertheless, there is often reason to avoid direct use of DNNs. For example, the training from scratch or hyperparameter tuning of such networks can be prohibitively expensive or time consuming (Schmitt et al. 2018). For some applications, the size or complexity of such DNNs precludes their use in real time, or employment in edge devices with limited processing resources (Chen et al. 2017), (Mirzadeh et al. 2019). In other areas such as flight control or self driving cars, DNNs are sidelined (at least for mass deployment) by their opaqueness or lack of decision making interpretability (Bastani, Kim, and Bastani 2017), (Hind et al. 2019).

In light of such issues, a vast body of work has focused in recent years on developing simpler or more structured controllers which retain desirable properties of a given DNN based controller (Bastani, Pu, and Solar-Lezama 2018). Additionally, multiple studies in this area, e.g., (Bastani, Pu, and Solar-Lezama 2018), (Ba and Caruana 2014) attribute the efficacy of DNNs across such a broad range of problems not to an inherently richer representative capacity over other

architectures, or even over shallower neural networks, but rather to the many regularization techniques which currently facilitate DNN training. Therefore, while it may not always be clear how to precisely obtain alternative controllers with performance similar to DNNs, it is theoretically possible, and therefore well-motivated, to do so.

A related challenge is how to select an alternative controller, given multiple objectives. For example, given a reference DNN, one may wish to design an alternative controller with fewer parameters and comparable performance that is also easier to understand. In this work, we propose a collection of metrics constituting a framework for evaluating how well decision tree controllers *distilled* from a target DNN “match” the original, as well as how to make comparisons amongst competing alternatives. We focus on reinforcement learning (RL) tasks, and in particular on decision tree alternatives to DNNs trained via the DQN algorithm. We study standard hard decision trees based on thresholding of input attributes at inner nodes as well as “soft” decision trees as described in (Frosst and Hinton 2017) and in later sections of this work.

We consider metrics such as the average reward, policy accuracy percentage, number of parameters, and normalized root mean square (NRMS) error between what we term the *empirical value functions* (EVFs) associated with each controller (including the reference DQN). To obtain the EVFs, we use sample trajectories starting from a collection of points spanning a given RL environment’s state space, since both hard and soft decision tree controllers do not directly provide such an estimate. Based on these metrics, we assess collections of hard and soft trees, demonstrating how a designer can tailor a controller to specific design criteria, in particular by tuning the tree depth. In summary, *our contributions* can be summarized as follows:

- We propose a collection of metrics including a novel, empirical value function based RMS distance metric for evaluating the quality of distilled hard and soft decision tree controllers;
- We train hard and soft decision trees of varying depth, and examine the impact of this parameter on our proposed distillation quality metrics.
- We demonstrate via our framework that in our test environment, approximately 80% accuracy in policy match-

ing yields performance comparable to the original DNN, and that the SDT achieving these thresholds does so with fewer parameters and NRMS error than the HDTs which reach the same accuracy and performance level.

2 Background

2.1 Related Work

Related literature can be broken into two primary areas: knowledge distillation and model evaluation metrics.

Knowledge distillation. In essence, distillation is the transfer of behavior or learned knowledge for a given problem or task from one model or controller to another. Briefly, this is related to, but distinct from *model compression*, which seeks to quantize, code or otherwise process reference network weights in a way that leads to a reduced complexity model of the same structure (Polino, Pascanu, and Alistarh 2018). Our framework could be used to evaluate the models resulting from such processes as well, but we focus here instead on distillation.

(Buciluá, Caruana, and Niculescu-Mizil 2006) train modestly sized models on “pseudo-data” generated by large ensembles of base level classifiers. This teacher-student paradigm is central to the distillation literature. (Ba and Caruana 2014) demonstrates that shallow neural networks can be trained to achieve comparable performance to state-of-the-art DNNs with the same number of parameters when the shallow networks are trained to mimic the DNNs instead of learning directly from the original labeled training data. Concentrating on edge devices such as smart phones, (Mirzadeh et al. 2019) demonstrate a student of fixed size or complexity will perform poorly if the teacher is too large, and propose a “teaching-assistant” facilitated process involving multiple distillation steps between the original teacher and target student.

(Hinton, Vinyals, and Dean 2015) argues that by training a student neural network using a weighted combination of the correct labels and the output soft labels (class probabilities) generated by a teacher network helps transfer knowledge to the student regarding relative likelihoods of different classes, therefore improving student performance. (Chen et al. 2017) extended this approach to more complex, multi-class object tasks by incorporating training loss functions accounting for class imbalance as well as “hints” from intermediate teacher layers, amongst other techniques. (Frosst and Hinton 2017) demonstrated that the target student need not be a smaller neural network, introducing *soft decision trees* (SDTs) which essentially feature a single layer perceptron at each inner node. Training these SDTs on data generated by an expert DNN improves performance over training directly on the labeled data. See Section 3 for a more detailed overview of this approach.

Distillation has also been extended from the realm of supervised learning to RL. Using a technique termed *policy distillation*, (Rusu et al. 2015) shows the policy of an RL agent can be extracted to train a smaller, more efficient network to perform at expert level. (Bastani, Pu, and Solar-Lezama 2018) augment the DAGGER algorithm (Ross, Gordon, and Bagnell 2011) by making use of the expert net-

work’s Q-function (see Section 2.1) to extract a series of policies, the best of which is selected based upon a cross-validation procedure. (Liu et al. 2018) extend mimic learning to RL settings via Linear Model U-Trees (LMUTs), a variant of the U-Tree (McCallum et al. 1996) representation of a Q function, placing linear models at each leaf node. Turning to a different objective, (Schmitt et al. 2018) proffer the *kickstarting* approach to speed up the training RL students in the presence of trained experts. Finally, (Coppens et al. 2019) studied how the SDTs described in (Frosst and Hinton 2017) can be used to explain the behavior of expert DNNs in an RL setting.

Evaluation metrics. The collection of controller evaluation metrics presented here is most closely related to (Andrews, Diederich, and Tickle 1995), which proposes four metrics to measure the quality of rules extracted from a neural network (Dancey, Bandar, and McLean 2007): accuracy, fidelity, consistency and comprehensibility. For a classifier \hat{c} , accuracy is defined in (Andrews, Diederich, and Tickle 1995) as

$$P(\hat{c}(X) = C),$$

where C represents a previously unseen problem instance. Fidelity, the extent to which the classifier \hat{c} decisions correspond to the original neural network (nn) is defined as the probability

$$P(\hat{c}(X) = nn(X)).$$

Consistency refers to the stability of the extracted policy across multiple nn training sessions, and comprehensibility is the number of rules extracted from the network, along with the number of antecedents or conditions per rule.

Accuracy is not applicable in our RL settings, but the notion of fidelity presented above aligns with the policy accuracy metric we introduce in Section 3. Given our focus on decision trees, comprehensibility corresponds to the figures we later present on number of tunable parameters, as each inner node in both hard and soft essentially represents a rule.

Our EVF based NRMS calculation is most closely related to the examination of mean absolute error (MAE) and root mean square error (RMSE) between reference DNN and LMUT Q function representations in (Liu et al. 2018). We instead examine the distance between empirical estimates for the *value* functions corresponding to each type of controller, as this captures in some sense the policy actually followed by each controller, given the system dynamics.

2.2 Reinforcement Learning

The technique of Reinforcement Learning (RL) (Bertsekas 2019) is intuitively best understood as trying to find a mapping from environment state observations to agent actions while learning about an unknown environment on the fly. Further, it is desired that the final mapping obtained yield the best possible result in terms of task completion and/or cumulative reward.

An RL environment is modeled as a Markov Decision Process (MDP), specified by the tuple (S, A, P, r, γ) :

1. S : *state space*, i.e., the set of possible states of the environment.

2. A : *action space*, i.e., the set of possible actions of the agent.
3. P : transition probability, where $P_a(s, s')$ is the probability of moving to state s' on taking action a in state s .
4. r : reward function where $r(s, a)$ is the reward obtained on taking action a in state s .
5. γ : *discount factor*, $0 < \gamma < 1$.

A *policy* $\pi : S \rightarrow A$ is a mapping from the state space to the action space, indicating the action an agent should take in a particular state.

The goal of reinforcement learning is to find a policy π which maximizes the *expected cumulative reward*, mathematically defined as

$$R = \mathbb{E} \left[\sum_{t=0}^{\infty} \gamma^t r(s_t, a_t) \right],$$

i.e., find π^* such that:

$$\pi^* \in \arg \max_{\pi} \mathbb{E} \left[\sum_{t=0}^{\infty} \gamma^t r(s_t, \pi(s_t)) \right]. \quad (1)$$

The *value function* $V^{\pi} : S \rightarrow \mathbb{R}$ associated with policy π gives the expected cumulative reward, starting from state s and following policy π :

$$V^{\pi}(s) = \mathbb{E} \left[\sum_{t=0}^{\infty} \gamma^t r_t \right] \quad \forall s \in S. \quad (2)$$

An *optimal value function* V^* satisfies

$$V^*(s) = \max_{\pi} V^{\pi}(s) \quad \forall s \in S, \quad (3)$$

and it can be shown that optimal policies as in (1) correspond to optimal value functions, i.e.,

$$\pi^* = \arg \max_{\pi} V^{\pi}(s) \quad \forall s \in S.$$

Q-learning. A standard algorithm for finding the optimal policy in (1) is the Q-learning algorithm which utilizes Q values defined for state action pairs. Under a given policy π , $Q^{\pi}(s, a)$ is defined as:

$$Q^{\pi}(s, a) = r(s, a) + \mathbb{E} \left[\sum_{t=1}^{\infty} \gamma^t r(s_t, \pi(s_t)) \right]. \quad (4)$$

Thus, $Q^{\pi}(s, a)$ gives the expected value of starting from state s , taking action a , and then taking actions following policy π for the rest of the time horizon. The optimal Q value function, $Q^*(s, a)$ is defined as:

$$Q^*(s, a) = \max_{\pi} Q^{\pi}(s, a). \quad (5)$$

Note that together (2), (3) and (4) give

$$V^*(s) = \max_a Q^*(s, a) \quad \forall s \in S,$$

and the optimal policy can be derived from the optimal Q value function Q^* as follows:

$$\pi^*(s) \in \arg \max_a Q^*(s, a) \quad \forall s \in S. \quad (6)$$

The *Q-learning algorithm* is a standard iterative algorithm for computation of the optimal Q value function. Each iteration is of the following nature:

$$Q'(s_t, a_t) \leftarrow Q(s_t, a_t) + \alpha_t (r(s_t, a_t) + \gamma \max_a Q(s_{t+1}, a) - Q(s_t, a_t)), \quad (7)$$

where Q' is the updated Q value, α_t is the *learning rate* and γ is the *discount factor*. The action a_t at each step t is typically ϵ -greedy with respect to the current Q values.

The above iterative algorithm has been proven (Bertsekas 2019) to converge to the optimal Q^* for suitable learning rates. This algorithm is an example of a *model-free* reinforcement learning algorithm, as the transition probabilities between states for a given action are not known and not taken into account in the algorithm. It is also an example of a *temporal difference* algorithm, where one *unrolls* the dynamics of the environment one step in the future and adjusts the current prediction to match it. For more details on the Q-learning algorithm in particular and RL in general, we refer the readers to (Bertsekas 2019), (Sutton and Barto 2018).

Deep Reinforcement Learning. The Q-learning algorithm for RL works well for small state-action spaces. However, even for the discrete state space setting, increasing the number of states leads to the well known curse of dimensionality issue, rendering direct application of Q-learning intractable, and suggesting the need for some sort of *approximation* of the Q -value function. Currently one of the most popular ways to approximate the Q -value function is to use a neural network. This is the key idea behind the technique of *deep reinforcement learning* (*deep RL*).

For a continuous state space and discrete action space, we use a *regressor* neural network which provides estimates of the Q -value function for every action at every state. Consequently, the optimal policy after training will involve selecting that action which gives the highest Q .

In this work, we consider deep RL policies obtained by using the DQN (Deep Q Network) algorithm. This algorithm expands on the Q-learning algorithm by the introduction of additional steps including experience replay and target network in order to stabilize learning. Further details can be obtained in (Mnih et al. 2013).

2.3 Imitation Learning

We use the methodology of *imitation learning* (Abbeel et al. 2007; Bain 1995) to train our simpler and more interpretable decision trees (students) to imitate the complex trained DQN (expert).

Behavioral cloning The simplest and most intuitive way to accomplish imitation learning is to *copy what the expert would do at the given state* by the way of *supervised learning*. The algorithm based on this straightforward idea is referred to as “behavioral cloning” (Bain 1995). In this algorithm, the expert plays the control task over several episodes, and the agent simply stores the demonstrations of the expert as state action pairs to which supervised learning is later applied (the state action pairs are considered as i.i.d).

2.4 Soft Decision Trees

While DNNs perform well in automatically learning policies for control problems, this efficacy is often offset by a lack of clarity as to how specific actions are selected. The root of this difficulty lies in the distributed nature of the representations embedded in the hidden layers of DNNs (Frosst and Hinton 2017). Beyond the first or last few layers, it is usually hard to explain the functional role of a given node as layers repeatedly aggregate latent features in order to form subsequent representations.

Decision trees offer an alternative, often more legible decision making paradigm. Decision tree selected actions can be traced back through sequences of decisions based directly on input data. In particular, we focus in this work on *soft decision trees* (SDTs), as described in (Frosst and Hinton 2017). For this class of binary decision trees, each inner node i learns a filter \mathbf{w}_i and bias b_i , in order to output a probability of taking the right branch

$$p_i(\mathbf{x}) = \sigma(\beta(\mathbf{x}^T \mathbf{w}_i + b_i)).$$

The parameter β , termed the ‘inverse temperature’, is introduced in order to avoid very soft decisions. The inverse temperature may be a learned parameter or static hyperparameter. Each leaf node ℓ learns a distribution over the possible output selections

$$Q_k^\ell = \frac{\exp(\phi_k^\ell)}{\sum_{k'} \exp(\phi_{k'}^\ell)}.$$

A simple two-leaf tree with this architecture is shown in Figure 1.

Learning occurs via mini-batch gradient descent. In our setting, the SDT learns based on environment state observations paired with actions from the expert DQN. The training makes use of a loss function which minimizes the cross entropy between each leaf and the target distribution T , weighted by its path probability

$$L(\mathbf{x}) = \log \left(- \sum_{\ell \in \text{leaf nodes}} P^\ell(\mathbf{x}) \sum_k T_k \log Q_k^\ell \right),$$

where T is the target distribution, and $P^\ell(\mathbf{x})$ is the probability of arriving at node ℓ , given input \mathbf{x} .

Unlike standard decision trees, this architecture allows for decisions to be made at each inner node based on aggregated input characteristics, rather than splitting based upon value ranges of input characteristics. Note that the input is fed directly into each inner node simultaneously, with the path from root to leaf for a given input being determined by left/right decisions at the inner nodes encountered. Having arrived at a leaf node, the output selection can be made either randomly according to the learned distribution, or by selecting the output with the highest probability at that leaf.

Empirically it has been shown (Frosst and Hinton 2017) that on supervised learning tasks such as MNIST digit recognition, SDTs trained on the outputs of a neural net expert exhibit better generalization than trees trained on data directly, though they do not match the performance of the expert.

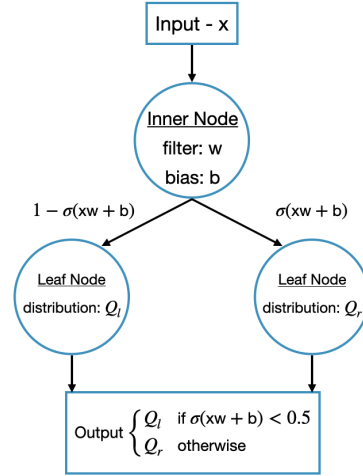


Figure 1: SDT with a single inner node and two leaf nodes (Frosst and Hinton 2017)

However, it is often easier to explain the output decisions of the SDTs than those of the neural network, as SDTs learn to make hierarchical decisions.

Our SDT implementation was based on the Github repository ‘Hierarchical mixture of Bigots’ (Martak 2020) associated with publication (Frosst and Hinton 2017). The case study environments were implemented using off-the-shelf implementations available in the OpenAI Gym software package (Brockman et al. 2016). All implementations of the hard and soft decision trees for these this test environment were carried out on a Macbook Pro with a Quad-Core Intel Core i5 processor and 8GB RAM.

3 Controller Characterization Metrics

Given a reference expert controller and a collection of distilled models, it is desirable to identify which of the models represents the ‘best’ approximation to the expert. Precise characterization of the quality of a distilled representation of the expert, i.e., which *metrics* should be used to evaluate the learned policies - remains application specific, and in many cases an open problem, particularly in applications focused on interpretability. Much recent work on distillation techniques and their application focuses on controller performance (Bastani, Pu, and Solar-Lezama 2018), (Coppens et al. 2019), (Frosst and Hinton 2017). In particular, (Liu et al. 2018) explicitly asserts that *play performance*, the average return achieved by the distilled controller is the most relevant metric. Indeed, in practice many of the studies cited in Section 2.1 simply take the highest performing controller as best, though not all, e.g. (Bastani, Kim, and Bastani 2017). Still, controller performance alone does not indicate the extent to which the distilled controller ‘matches’ or explains the target DNN policy, particularly in cases where fitted models have lower performance than the expert (Coppens et al. 2019). Aside from performance, *fidelity*, or the extent to which fitted models match the predictions of the expert is another natural evaluation metric for distilled mod-

els (Liu et al. 2018).

We evaluate decision trees distilled from a reference DNN based upon controller performance means and confidence bounds, as well as a pair of fidelity metrics. Taking the view of both the reference DNN and distilled trees as function approximators for the true value function of a given environment, we examine the normalized RMS error between the *empirical value functions* associated with each model.

Figure 2 illustrates the generation and comparison of these empirical value functions. The reference DNN can be represented by the function, \tilde{Q} . Given distillation training observation set (states) $s_{\text{train}} = \{s_1, \dots, s_n\}$, with $n \in \mathbb{Z}$, the DNN outputs corresponding labels (actions) $\tilde{a} = \{\tilde{a}_1, \dots, \tilde{a}_n\}$. Together, labeled data (s, \tilde{a}) is used to train a soft decision tree as detailed in Section 2.4. We infer policies $\tilde{\pi}$ and $\hat{\pi}$ corresponding to the DNN and SDT, respectively as discussed in Sections 2.2 and 2.4. Starting from randomly seeded starting states $s_{\text{test}} = \{s'_1, \dots, s'_m\}$ with $m \in \mathbb{Z}$, trajectories for both the DNN and SDT are generated in order to obtain empirical estimates of the value functions $\hat{V}_{\tilde{\pi}}$ and $\hat{V}_{\hat{\pi}}$ associated with $\tilde{\pi}$ and $\hat{\pi}$, respectively. We then take the empirical L2 norm of the difference between $\hat{V}_{\tilde{\pi}}$ and $\hat{V}_{\hat{\pi}}$, evaluated at s_{test} and normalized by the maximum absolute value of $\hat{V}_{\hat{\pi}}$:

$$\text{RMSE}(\hat{V}_{\tilde{\pi}}, \hat{V}_{\hat{\pi}}, s_{\text{test}}) = \sqrt{\frac{1}{m} \sum_{s' \in s_{\text{test}}} (\hat{V}_{\tilde{\pi}}(s') - \hat{V}_{\hat{\pi}}(s'))^2}$$

$$\text{NRMSE}(\hat{V}_{\tilde{\pi}}, \hat{V}_{\hat{\pi}}, s_{\text{test}}) = \frac{\text{RMSE}(\hat{V}_{\tilde{\pi}}, \hat{V}_{\hat{\pi}}, s_{\text{test}})}{\max_s |\hat{V}_{\hat{\pi}}(s)|}. \quad (8)$$

We focus here on value function approximation, rather than Q-value function approximation, as the value function reflects the actions that are actually taken under a given policy, and therefore captures in some sense the closed loop behavior of the controllers under comparison.

The second fidelity metric that we consider is policy accuracy, or percent 0-1 loss, which we later report as the percentage

$$\% \text{ACC}(\tilde{\pi}, \hat{\pi}, s_{\text{grid}}) = \frac{|\{s \in s_{\text{grid}} : \tilde{\pi}(s) = \hat{\pi}(s)\}|}{|\{s \in s_{\text{grid}}\}|},$$

where s_{grid} is a discretization of S .

Policy accuracy is meant to assess how well the actions taken under a distilled tree policy $\hat{\pi}$ match the actions of the reference DNN. Intuitively, fixing a tree depth n , a more accurate distilled tree should provide a better explanation of the latent knowledge captured in the DNN.

Aside from performance and fidelity, we also consider the complexity of candidate controllers in terms of the number of included trainable parameters.

4 Case Study

In this section, we detail case studies for the MountainCar-v0 and Cartpole-v0 OpenAI Gym environments.

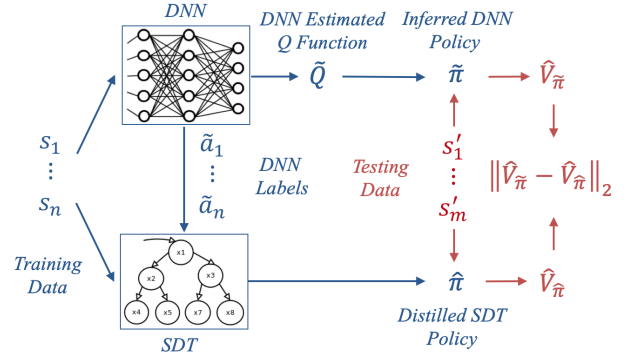


Figure 2: Generation and L2 norm comparison of empirical value functions $\hat{V}_{\tilde{\pi}}$ and $\hat{V}_{\hat{\pi}}$.

4.1 Mountain Car Problem

Problem description. The mountain car problem is a well-known benchmark problem in reinforcement learning, prevalent in the literature since the 1990s (Moore 1990). The problem includes an under powered mountain car trying to reach a hilltop, starting out from a valley. As the car lacks sufficient power to drive directly uphill to the goal, the policy that suits it the best is to reverse up the hill on the opposite side and use the acquired momentum in addition to the engine to reach the goal location.

In this problem, the state space is continuous with two states – the position of the car along the x -axis, contained in the interval $[-1.2, 0.6]$, and the velocity of the car, contained in the interval $[-0.07, 0.07]$. Three actions are allowed – the car can either choose to go left, go right or do nothing. The task is declared successfully completed if the car reaches the goal state within 200 time steps. For every time step that the goal is not reached, the car receives a reward of -1 point. The episode is terminated as a failure if the time limit is exceeded and the car has not reached its goal.

Expert DQN. For MountainCar-v0, our expert neural net consisted of two hidden layers with 24 and 48 neurons, and three output neurons to account for the three possible actions. Discount factor γ was set to 0.99 for training, and this architecture was trained using the DQN algorithm on 400 episodes of MountainCar-v0. The output reference model has a total of 1419 trainable parameters. The DQN learned the optimal control policy successfully. We tested the DQN controller over 100 episodes, and observed that the controller succeeded in achieving the goal in every episode. The DQN completed the control task over all the 100 episodes with a mean cumulative reward and 95% confidence interval of -154.05 ± 0.79 units.

Both soft and hard trees were trained on a set of labeled data generated by the expert DQN over 1500 MountainCar-v0 episodes. The data was preprocessed such that the final distillation data contained equal numbers of state/actions pairs for each of the three available actions. In all, the distillation training set contained 167,085 data points.

Hard and soft decision trees. Soft decision trees of depths 2 through 9 were trained using the technique discussed in Section 2.4. Hard trees of depths 2 through 9 were trained on the DQN generated labeled data using the sklearn Python package (Pedregosa et al. 2011).

Figure 3 shows a trained SDT of depth 3. The colored squares in the inner layer nodes display the trained weights w_i . At each inner node, the left half panel gives the weight applied to the car position, while the right half panel gives the weight applied to the car velocity. Thus, for example, one may observe that the decision made at the root node depends most heavily on the (signed) car velocity. The tricolor panels at the leaf nodes represent the learned probability distribution over potential actions, with the letter corresponding to highest probability action given for each leaf node in the bottom row. For this particular tree, there is a clear highest probability action corresponding to each leaf node.

Figures 4 through 7 display the results of the application of the metrics introduced in Section 3 to the sets of hard and soft trees, and reference DQN. Starting with our fidelity metrics, Figure 4 compares the NRMS values as calculated in (8) for each tree type and depth. For the purposes of this plot, the state space was discretized to 20 steps in each dimension, giving 400 test trajectories overall for each controller. As can be seen, the L2 error does not vary considerably with the tree depth for trees of either type, though the error increases slightly with depth for hard trees.

Figure 5 shows the policy accuracy percentage for each of the distilled controller. In this experiment, the state space was discretized more finely, as each data point requires a call to the controller’s prediction function, rather than a complete episode trajectory. In particular, the range of each input state feature was discretized into 100 steps. For the tree depths tested, depth 5 gives the optimal accuracy for SDTs, as deeper, more complex trees appear to overfit to the DQN labeled data. On the other hand, in terms of percentage policy accuracy, HDTs increase monotonically with depth over the range tested.

Turning to performance, Figure 6 plots the empirical mean and 95% confidence intervals across 100 test trajectories for each controller. The DQN outperforms all SDTs in terms of mean reward, though the 95% confidence bounds of the depth 5 SDT overlap with those of the DQN. HDTs of depth 7 or greater either slightly outperform or essentially match the DQN.

Finally, Figure 7 compares the complexity of each distilled tree and the reference DQN in terms of tunable parameters. For each SDT, this number represents the learned weights and biases of each inner node, along with the probability distributions of each leaf node. For each HDT, this number is twice the number of inner nodes, as each inner node splits the data based upon an input attribute and threshold. For tree depth larger than 7, the SDTs actually become more complex than the DQN in the sense just described. The highest performing, depth 5 SDT is specified by 190 parameters, meaning this tree requires about 13% of the parameters needed to specify the DQN. The HDTs of depth 7, 8 and 9, which outperform this depth 5 SDT require 330, 446, and 570 parameters, respectively.

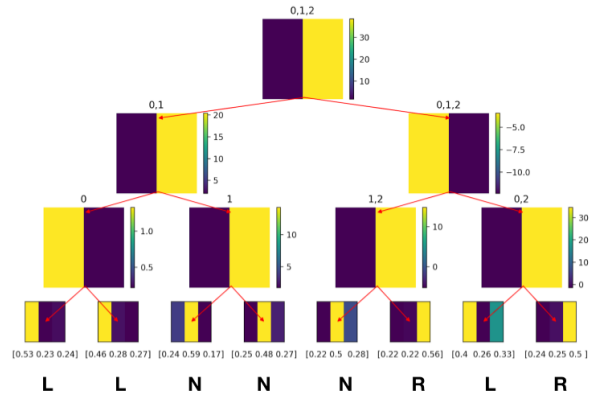


Figure 3: Soft Decision Tree for Mountain Car

For reference, Figures 8 and 9 show the policies associated with depth 2, 5 and 8 SDTs and HDTs, respectively, along with the DQN policy. Each policy plot again reflects discretization of the statespace S into 100 points along both position and velocity dimensions. As these plots demonstrate, while SDTs approximate the DQN policy via increasing number of hyperplanes, the HDTs approximate the DQN policy via increasingly finer simple functions.

See the Supplementary Materials for a similar analysis in the context of the CartPole-v0 environment, another benchmark problem available as part of the OpenAI Gym toolkit.

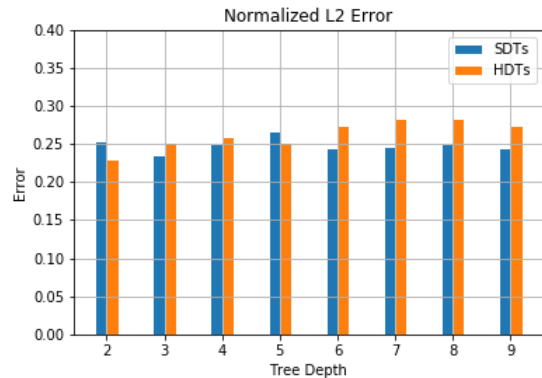


Figure 4: Normalized RMS L2 Error for Mountain Car HDT/SDTs depth 2-9 (statespace discretized into 20 steps per dimension).

Discussion. Overall, we identify three primary takeaways from our case study. First, larger tree depth does not always result in improved performance or fidelity. Second, given our choice of decision tree architecture and training methodology, as well as RL environment, it seems that the percentage accuracy is a better predictor of performance than the proposed L2 error metric. Third, soft decision trees with a fraction of the tunable parameters of the original DNN can achieve similar performance in the MountainCar-v0 task.

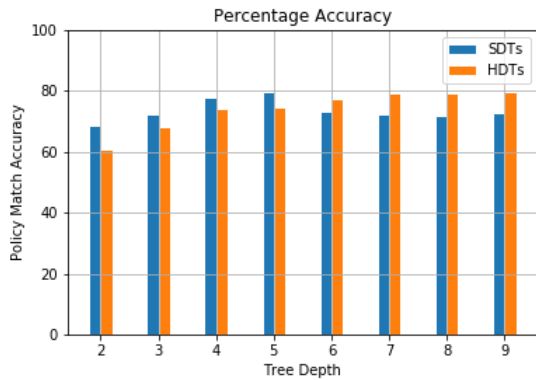


Figure 5: Percentage Policy Accuracy for Mountain Car HDT/SDTs depth 2-9 (statespace discretized into 100 steps per dimension).

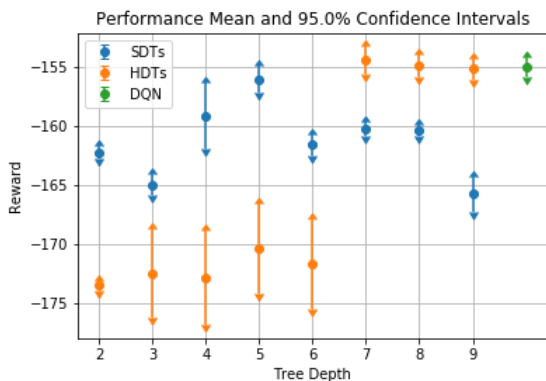


Figure 6: Performance evaluation for Mountain Car HDT/SDTs and reference DQN over 100 episodes.

4.2 Cart Pole Problem

Problem description. The cart pole problem is another benchmark problem in reinforcement learning (Barto, Sutton, and Anderson 1983). The specific version of the problem implemented in the CartPole-v0 OpenAI-Gym environment and studied here includes a pole attached to a cart via an un-actuated joint. The cart moves along a frictionless track, attempting to maintain the pole’s initial upright position.

The state space is continuous, with four elements: cart position, cart velocity, pole angle (measured from vertical with positive angles to the right) and pole velocity (measured at the tip). The cart position is contained within the interval $[-2.4, 2.4]$, while the pole angle is contained in the interval $[-41.2^\circ, 41.2^\circ]$. Both cart and pole angle velocities may take on any real value. Each state attribute is initialized to a uniformly distributed value in range $[-0.05, 0.05]$. Two actions are available, push left or push right. Episodes terminate when either the absolute value of the pole angle exceeds 12° , the cart position reaches ± 2.4 , or the episode lasts 200 time steps. The reward is 1 for each time step taken.

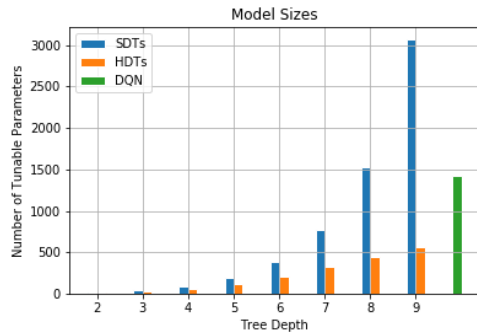


Figure 7: Number of parameters for Mountain Car HDT/SDTs and reference DQN.

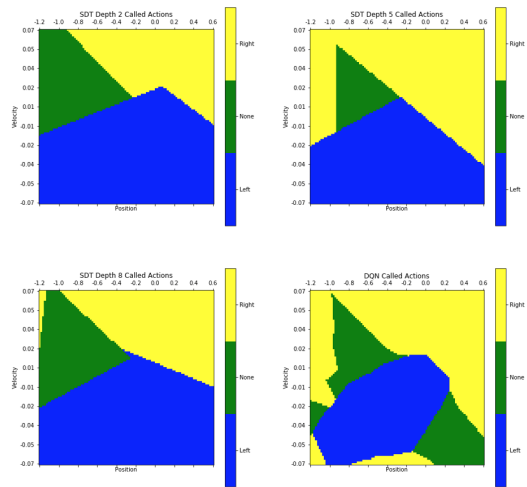


Figure 8: Trained Mountain Car SDT and DQN policies, for statespace S discretized to 10000 points.

Expert DQN. For CartPole-V0, our neural network included 4 dense layers, giving 38,531 trainable parameters overall. We used a baseline DQN framework from the OpenAI Gym baselines package (Dhariwal et al. 2017) for implementing the DQN algorithm. We tested the DQN controller over 100 episodes, and observed that the controller succeeded in obtaining the maximum possible reward of 200 in each episode.

Both soft and hard trees were trained on a set of labeled data generated by the expert DQN over 750 CartPole-v0 episodes. The data was preprocessed such that the final distillation data contained equal numbers of state/actions pairs for each of the two available actions. In all, the distillation training set contained 148,452 data points.

Hard and soft decision trees. Soft decision trees (SDTs) of depths 2 through 9 were trained using the technique discussed in (Frosst and Hinton 2017). Hard decision trees (HDTs) of depths 2 through 9 were trained on the DQN generated labeled data using the sklearn Python package (Pedregosa et al. 2011).

Figure 10 shows a trained SDT of depth 3. The colored

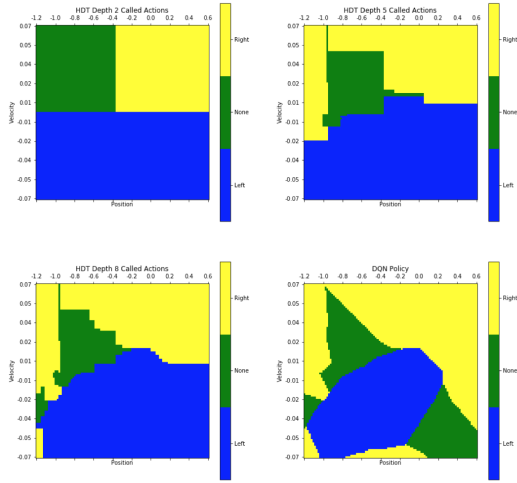


Figure 9: Trained Mountain Car HDT and DQN policies, for statespace S discretized to 10000 points.

squares in the inner layer nodes display the trained weights w_i . At each inner node, the four panels give the weight applied to each input feature, in the order described above, from left to right. Thus, for example, one may observe that the decision made at the root node depends most heavily on the pole angle. The two-color panels at the leaf nodes represent the learned probability distribution over potential actions, with the letter corresponding to highest probability action given for each leaf node in the bottom row. For this particular tree, there is a clear highest probability action corresponding to each leaf node, aside from the third from the left.

Figures 11 through 14 display the results of the application of the metrics introduced in Section 3 of the primary submission to the sets of hard and soft trees, and reference DQN. Starting with our fidelity metrics, Figure 4 compares the NRMS values as calculated according to

$$\text{RMSE}(\widehat{V}_{\pi}, \widehat{V}_{\pi}, s_{\text{test}}) = \sqrt{\frac{1}{m} \sum_{s' \in s_{\text{test}}} (\widehat{V}_{\pi}(s') - \widehat{V}_{\pi}(s'))^2}$$

$$\text{NRMSE}(\widehat{V}_{\pi}, \widehat{V}_{\pi}, s_{\text{test}}) = \frac{\text{RMSE}(\widehat{V}_{\pi}, \widehat{V}_{\pi}, s_{\text{test}})}{\max_s |\widehat{V}_{\pi}(s)|}$$

for each tree type and depth. For the purposes of this plot, the state space was discretized to 5 steps in each dimension, giving 625 test points overall. The cart position was discretized across $[-2.4, 2.4]$, while the pole angle was discretized across $[-12^\circ, 12^\circ]$, i.e., the nonterminating values. Both cart and pole velocities were limited to range $[-0.05, 0.05]$. As can be seen, for both types of trees the error generally decreases with tree depth up to depth 8.

Figure 5 shows the policy accuracy percentage for each of the distilled controller. In this experiment, the state space was discretized more finely, as each data point requires a call to the controller’s prediction function, rather than a complete episode trajectory. In particular, the range of each input state

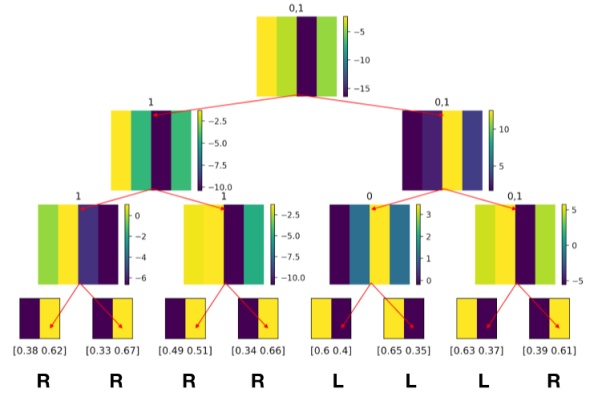


Figure 10: Soft Decision Tree for Cart Pole

feature was discretized into 10 steps, over the ranges mentioned in the preceding paragraph. For the tree depths tested, depth 9 gives the optimal accuracy for SDTs. On the other hand, percentage policy accuracy remains essentially constant for HDTs.

Turning to performance, Figure 6 plots the empirical mean and 95% confidence intervals across 100 test trajectories for each controller. Trees of both types are successful in matching the performance of the DQN. All but depth 3 HDTs achieve the maximum reward of 200, along with SDTs of depth 2 through 5, as well as 7, within confidence bounds.

Finally, Figure 7 compares the complexity of each distilled tree and the reference DQN in terms of tunable parameters. The DQN parameter count far exceeds any tree tested, and thus is omitted. For each SDT, this number represents the learned weights and biases of each inner node, along with the probability distributions of each leaf node. For each HDT, this number is twice the number of inner nodes, as each inner node splits the data based upon an input attribute and threshold. The smallest SDT to achieve a mean reward of 200, depth 3, is specified by 52 parameters, while the smallest HDT to achieve this mean is specified by just 6 parameters.

Discussion. For the CartPole-v0 task, the clearest correspondence between metrics comes in the case of HDTs, where essentially uniform accuracy across tree depth aligns with basically uniform performance across tree depth. Within confidence bounds, SDTs which exceed the HDT level of accuracy also match the DQN performance level, aside from depth 6. It is important again note that each episode is initialized uniformly in the range $[-0.05, 0.05]$ for each state attribute, meaning that the range of states examined for both L2 error and percentage accuracy likely exceeds the range of states encountered by the reference DQN, as well as other high performing controller. This may explain the lack of obvious correspondence between performance and either of these metrics in SDTs, and HDTs in the case of L2 error, as many states tested may not be encountered often in actual trajectories. Finally, both soft and

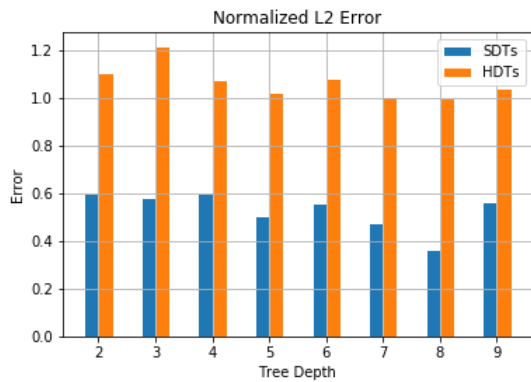


Figure 11: Normalized RMS L2 Error for Cart Pole HDT/SDTs depth 2-9 (statespace discretized into 20 steps per dimension).

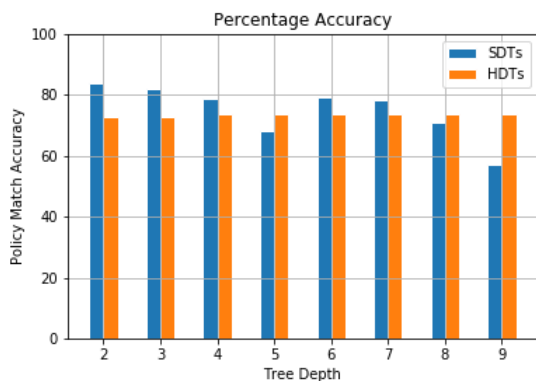


Figure 12: Percentage Policy Accuracy for Cart Pole HDT/SDTs depth 2-9 (statespace discretized into 10 steps per dimension).

hard decision trees with a fraction of the tunable parameters of the original DNN can achieve similar performance in the CartPole-v0 task.

5 Conclusion and Future Work

We introduced an evaluation framework and metrics to assess the quality of distilled decision tree controllers in RL settings against a variety of design objectives. Specifically, we consider normalized root mean square error between empirical value functions, policy match accuracy, mean performance with confidence bounds, and number of tunable parameters to guide designers and researchers toward assessing tradeoffs between performance, fidelity, and complexity as tree depths and types vary.

Future directions for our work include: Considering alternative architectures beyond trees, such as kernel machines; Incorporating more sophisticated learning algorithms such as DAGGER (Ross, Gordon, and Bagnell 2011) into the training of our alternative architectures; and develop metrics which focus more on the “closed-loop” behavior of con-

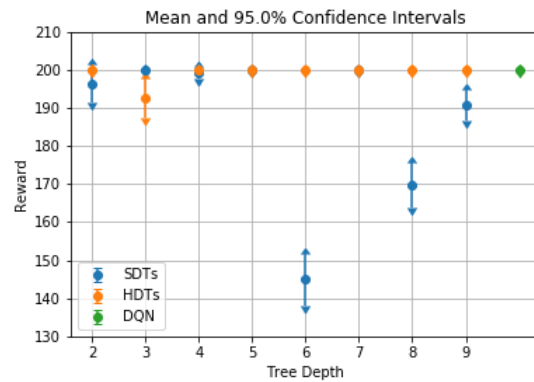


Figure 13: Performance evaluation for Cart Pole HDT/SDTs and reference DQN for 100 episodes.

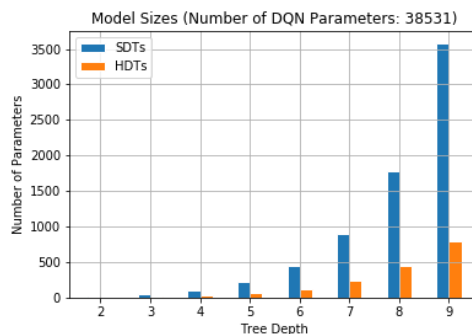


Figure 14: Number of parameters for Cart Pole HDT/SDTs and reference DQN.

trollers in a given environment.

References

- Abbeel, P.; Coates, A.; Quigley, M.; and Ng, A. Y. 2007. An application of reinforcement learning to aerobatic helicopter flight. In *Advances in neural information processing systems*, 1–8.
- Andrews, R.; Diederich, J.; and Tickle, A. B. 1995. Survey and critique of techniques for extracting rules from trained artificial neural networks. *Knowledge-based systems* 8(6): 373–389.
- Ba, J.; and Caruana, R. 2014. Do deep nets really need to be deep? In *Advances in neural information processing systems*, 2654–2662.
- Bain, M. 1995. A Framework for Behavioural Cloning. In *Machine Intelligence 15*, 103–129.
- Barto, A. G.; Sutton, R. S.; and Anderson, C. W. 1983. Neuronlike adaptive elements that can solve difficult learning control problems. *IEEE transactions on systems, man, and cybernetics* (5): 834–846.
- Bastani, O.; Kim, C.; and Bastani, H. 2017. Interpretability via model extraction. *arXiv preprint arXiv:1706.09773*.

- Bastani, O.; Pu, Y.; and Solar-Lezama, A. 2018. Verifiable reinforcement learning via policy extraction. In *Advances in neural information processing systems*, 2494–2504.
- Bertsekas, D. P. 2019. *Reinforcement learning and optimal control*. Athena Scientific.
- Brockman, G.; Cheung, V.; Pettersson, L.; Schneider, J.; Schulman, J.; Tang, J.; and Zaremba, W. 2016. Openai gym. *arXiv preprint arXiv:1606.01540*.
- Buciluă, C.; Caruana, R.; and Niculescu-Mizil, A. 2006. Model compression. In *Proceedings of the 12th ACM SIGKDD international conference on Knowledge discovery and data mining*, 535–541.
- Chen, G.; Choi, W.; Yu, X.; Han, T.; and Chandraker, M. 2017. Learning efficient object detection models with knowledge distillation. In *Advances in Neural Information Processing Systems*, 742–751.
- Coppens, Y.; Efthymiadis, K.; Lenaerts, T.; and Nowe, A. 2019. Distilling deep reinforcement learning policies in soft decision trees. In *Proceedings of the IJCAI 2019 Workshop on Explainable Artificial Intelligence*, 1–6.
- Dancey, D.; Bandar, Z. A.; and McLean, D. 2007. Logistic model tree extraction from artificial neural networks. *IEEE Transactions on Systems, Man, and Cybernetics, Part B (Cybernetics)* 37(4): 794–802.
- Dhariwal, P.; Hesse, C.; Klimov, O.; Nichol, A.; Plappert, M.; Radford, A.; Schulman, J.; Sidor, S.; Wu, Y.; and Zhokhov, P. 2017. OpenAI Baselines. <https://github.com/openai/baselines>.
- Frosst, N.; and Hinton, G. 2017. Distilling a neural network into a soft decision tree. *arXiv preprint arXiv:1711.09784*.
- Hind, M.; Wei, D.; Campbell, M.; Codella, N. C. F.; Dhurandhar, A.; Mojsilovic, A.; Ramamurthy, K. N.; and Varshney, K. R. 2019. TED: Teaching AI to Explain its Decisions. In Conitzer, V.; Hadfield, G. K.; and Vallor, S., eds., *Proceedings of the 2019 AAAI/ACM Conference on AI, Ethics, and Society, AIES 2019, Honolulu, HI, USA, January 27-28, 2019*, 123–129. ACM. doi:10.1145/3306618.3314273. URL <https://doi.org/10.1145/3306618.3314273>.
- Hinton, G.; Vinyals, O.; and Dean, J. 2015. Distilling the knowledge in a neural network. *arXiv preprint arXiv:1503.02531*.
- Liu, G.; Schulte, O.; Zhu, W.; and Li, Q. 2018. Toward interpretable deep reinforcement learning with linear model utrees. In *Joint European Conference on Machine Learning and Knowledge Discovery in Databases*, 414–429. Springer.
- Martak, L. 2020. Distill-NN-Tree. URL <https://github.com/lmartak/distill-nn-tree>.
- McCallum, A. K.; et al. 1996. Learning to use selective attention and short-term memory in sequential tasks. In *From animals to animats 4: proceedings of the fourth international conference on simulation of adaptive behavior*, volume 4, 315. MIT Press.
- Mirzadeh, S.-I.; Farajtabar, M.; Li, A.; Levine, N.; Matsukawa, A.; and Ghasemzadeh, H. 2019. Improved Knowledge Distillation via Teacher Assistant. *arXiv preprint arXiv:1902.03393*.
- Mnih, V.; Kavukcuoglu, K.; Silver, D.; Graves, A.; Antonoglou, I.; Wierstra, D.; and Riedmiller, M. 2013. Playing atari with deep reinforcement learning. *arXiv preprint arXiv:1312.5602*.
- Moore, A. W. 1990. Efficient memory-based learning for robot control.
- Pedregosa, F.; Varoquaux, G.; Gramfort, A.; Michel, V.; Thirion, B.; Grisel, O.; Blondel, M.; Prettenhofer, P.; Weiss, R.; Dubourg, V.; Vanderplas, J.; Passos, A.; Cournapeau, D.; Brucher, M.; Perrot, M.; and Duchesnay, E. 2011. Scikit-learn: Machine Learning in Python. *Journal of Machine Learning Research* 12: 2825–2830.
- Polino, A.; Pascanu, R.; and Alistarh, D. 2018. Model compression via distillation and quantization. *arXiv preprint arXiv:1802.05668*.
- Ross, S.; Gordon, G.; and Bagnell, D. 2011. A reduction of imitation learning and structured prediction to no-regret online learning. In *Proceedings of the fourteenth international conference on artificial intelligence and statistics*, 627–635.
- Rusu, A. A.; Colmenarejo, S. G.; Gulcehre, C.; Desjardins, G.; Kirkpatrick, J.; Pascanu, R.; Mnih, V.; Kavukcuoglu, K.; and Hadsell, R. 2015. Policy distillation. *arXiv preprint arXiv:1511.06295*.
- Schmitt, S.; Hudson, J. J.; Zidek, A.; Osindero, S.; Doersch, C.; Czarnecki, W. M.; Leibo, J. Z.; Kuttler, H.; Zisserman, A.; Simonyan, K.; et al. 2018. Kickstarting deep reinforcement learning. *arXiv preprint arXiv:1803.03835*.
- Sutton, R. S.; and Barto, A. G. 2018. *Reinforcement learning: An introduction*. MIT press.